

Measurement-Based Entanglement Distillation and Constant-Rate Quantum Repeaters over Arbitrary Distances

Yu Shi,^{1,2,3,*} Ashlesha Patil,^{2,3} and Saikat Guha^{1,2,3,†}

¹*Department of Electrical and Computer Engineering,
University of Maryland, College Park, MD 20742, USA*

²*NSF-ERC Center for Quantum Networks, University of Arizona, Tucson, AZ 85721, USA*

³*Wyant College of Optical Sciences, University of Arizona, Tucson, AZ 85721, USA*

(Dated: February 18, 2025)

Measurement-based quantum repeaters employ entanglement distillation and swapping across links using locally prepared resource states of minimal size and local Bell measurements. In this paper, we introduce a systematic protocol for measurement-based entanglement distillation and its application to repeaters that can leverage any stabilizer code. Given a code, we explicitly define the corresponding resource state and derive an error-recovery operation based on all Bell measurement outcomes. Our approach offers deeper insights into the impact of resource state noise on repeater performance while also providing strategies for efficient preparation and fault-tolerant preservation of resource states. As an application, we propose a measurement-based repeater protocol based on quantum low-density parity-check (QLDPC) codes, enabling constant-yield Bell state distribution over arbitrary distances. Numerical simulations confirm exponential suppression of infidelity with increasing code size while maintaining a fixed code rate. This work establishes a scalable backbone for future global-scale fault-tolerant quantum networks.

Introduction.— Entanglement plays a crucial role in quantum networks [1–4], quantum metrology [5–8], and distributed quantum computing [9–13]. Establishing entanglement over long-range noisy channels requires quantum repeaters [14–17], which correct noise and relay entanglement over intervals. Since entanglement distillation and quantum error correction correspond one-to-one [18–21], repeaters based on both can be fundamentally unified using quantum error correction theory. Conventional repeaters apply error-correcting circuits directly to input qubits, which requires substantial auxiliary qubits and operations. In contrast, *measurement-based* repeaters use the principles of measurement-based quantum computing [22], and rely solely on local Bell measurements and entangled resource states [23], offering a simpler approach. Moreover, resource states can be prepared offline and locally, making this method well suited for modular qubit platforms such as trapped ions [24–26], reconfigurable ones such as neutral atoms [27–30], and qubit platforms lacking direct qubit-qubit interactions, such as photons [31–33] and color centers [34, 35].

Zwinger *et al.* [23, 36] proposed measurement-based quantum repeaters, deriving resource states by mapping unitary encoding circuits onto states via channel-state duality [37]. However, this approach incurs a high complexity of resource states and post-processing, thereby limiting its applicability to simple codes. They later introduced a hashing-based repeater protocol that enables a constant yield over any distance [38], but the proposal remains conceptual, lacking explicit resource states or error correction methods. Without a systematic framework, extending measurement-based quantum repeaters

to high-performance codes remains challenging, hindering their practical implementation.

In this paper, we systematically extend measurement-based entanglement distillation and develop an associated repeater protocol, supported by any stabilizer code. Using the parity-check matrix of a code, we explicitly define the resource state and present an error-recovery operation based on Bell measurement outcomes. Our resource states correspond to physical-logical Bell states (for distillation), and logical-logical Bell states (for repeaters). Their distillation capability can be evaluated using simple quantum error correction simulations. Resource state preparation simplifies to locally encoding logical Bell states, producible with constant circuit depth for certain codes, such as quantum low-density parity-check (QLDPC) codes [39]. Additionally, their preservation is achieved via syndrome error correction for logical qubits and distillation of local physical-logical entanglement, offering greater efficiency than the graph state distillation approach [40]. As an application, we propose a repeater protocol based on QLDPC codes, enabling constant-yield Bell state distribution over any distance with efficient resource state preparation. Numerical simulations demonstrate exponential infidelity suppression with increasing code size while maintaining a fixed encoding rate. Our protocol ensures efficiency and scalability, laying the foundation for global-scale quantum networks.

Measurement-based entanglement distillation.— We consider an $[[n, k, d]]$ -quantum error-correcting code with binary check matrix $\mathbf{H} = (\mathbf{H}_1 | \mathbf{H}_2)$ [41]. The steps of the measurement-based entanglement distillation protocol based on this code are outlined below, with a schematic shown in Figure 1 for illustration.

Step 1: Alice and Bob prepare their resource states, i.e.,

* shiyuphys@gmail.com

† saikat@umd.edu

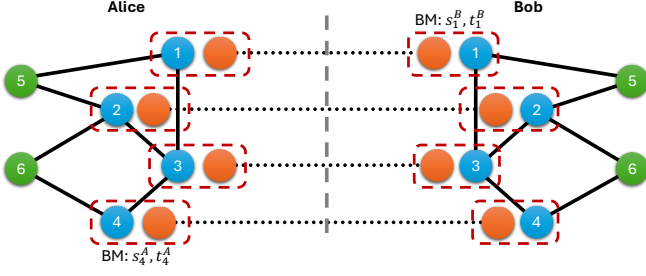


FIG. 1. Schematic of measurement-based entanglement distillation using the $[[4, 2, 2]]$ code with parity checks $X_1X_2X_3X_4$ and $Z_1Z_2Z_3Z_4$. The 6-qubit stabilizer states, drawn in graph states [43], process 4 noisy Bell states into 2 distilled Bell states. Blue circles denote interfacing qubits, green circles denote output qubits, and orange circles denote input Bell states. Dashed red rectangles indicate Bell measurements (BMs) with parities $s_i^{A(B)}$ for XX and $t_i^{A(B)}$ for ZZ .

an $(n+k)$ -qubit stabilizer state with generators

$$\{g_i, \bar{X}_j X_{n+j}, \bar{Z}_j Z_{n+j}\}. \quad (1)$$

Here, g_i represents the code stabilizer generator, where $i = 1, 2, \dots, n-k$. The code has supports on the first n qubits. \bar{X}_j and \bar{Z}_j represent the Pauli operators of the j -th logical qubit, X_{n+j} and Z_{n+j} represent the Pauli operators of the $(n+j)$ -th physical qubit, where $j = 1, 2, \dots, k$. $\bar{X}_j X_{n+j}$ and $\bar{Z}_j Z_{n+j}$ denote the tensor products $\bar{X}_j \otimes X_{n+j}$ and $\bar{Z}_j \otimes Z_{n+j}$, respectively. The resource state forms k logical-physical Bell states, represented by

$$|\mathcal{R}_D\rangle = \frac{1}{\sqrt{2^k}} \bigotimes_{j=1}^k (|\bar{0}_j\rangle |0_{n+j}\rangle + |\bar{1}_j\rangle |1_{n+j}\rangle), \quad (2)$$

where $\bar{0}_j$ and $\bar{1}_j$ represent the computational bases of the j -th logical qubit, and 0_{n+j} and 1_{n+j} represent the bases of the $(n+j)$ -th physical qubit.

Step 2: Alice and Bob each receive n input qubits, prepared as pairs in the standard Bell state

$$|\Phi^+\rangle = \frac{1}{\sqrt{2}} (|00\rangle + |11\rangle),$$

but have undergone noise before their delivery. Alice performs Bell measurements on the qubits she received and the first n qubits of her resource state. These measurements yield outcomes (s_i^A, t_i^A) , where s_i^A is the parity of the XX -measurement and t_i^A is the parity of the ZZ -measurement, for $i = 1, 2, \dots, n$. Bob mirrors Alice's operations, obtaining outcomes (s_i^B, t_i^B) .

Step 3: Alice sends her measurement results to Bob, who calculates the overall parities, represented by vectors \mathbf{s} and \mathbf{t} , with entries given by $s_i = s_i^A + s_i^B$

and $t_i = t_i^A + t_i^B$, respectively. Bob then computes the error syndrome by

$$\mathbf{S} = \mathbf{H}_1 \cdot \mathbf{s} + \mathbf{H}_2 \cdot \mathbf{t} + \mathbf{r}, \quad (3)$$

where \mathbf{r} , with

$$r_i = \sum_{j=1}^n H_1(i, j) H_2(i, j),$$

compensates for the effects of Pauli- Y operators in the code stabilizers. Note that all addition in this protocol is performed modulo 2.

Step 4: Using the error syndrome \mathbf{S} , Bob employs a decoder to estimate the noise $\hat{\mathbf{e}}$, as in conventional quantum error correction, and identifies the effective unilateral bit and phase flips on his output qubits. The bit flips are calculated by

$$\boldsymbol{\beta} = (\mathbf{Z}, \hat{\mathbf{e}})_{\text{sp}} + \mathbf{Z}_1 \cdot \mathbf{s} + \mathbf{Z}_2 \cdot \mathbf{t} + \mathbf{r}^b, \quad (4)$$

where $\mathbf{Z} = (\mathbf{Z}_1 | \mathbf{Z}_2)$ represents the binary matrix of logical Z operators, and $(\mathbf{Z}, \hat{\mathbf{e}})_{\text{sp}}$ is the symplectic inner product [42], representing the error-induced bit flips. The remaining terms represent the measurement-induced bit flips. The term \mathbf{r}^b , with

$$r_i^b = \sum_{j=1}^n Z_1(i, j) Z_2(i, j),$$

compensates for the effects of Pauli- Y operators. The phase flips are computed similarly by

$$\boldsymbol{\phi} = (\mathbf{X}, \hat{\mathbf{e}})_{\text{sp}} + \mathbf{X}_1 \cdot \mathbf{s} + \mathbf{X}_2 \cdot \mathbf{t} + \mathbf{r}^p, \quad (5)$$

where $\mathbf{X} = (\mathbf{X}_1 | \mathbf{X}_2)$ represents the binary matrix of logical X operators, and the elements of \mathbf{r}^p ,

$$r_i^p = \sum_{j=1}^n X_1(i, j) X_2(i, j).$$

Step 5: Bob corrects the bit and phase flips by applying appropriate Pauli gates on his $(n+i)$ -th qubit, transforming (β_i, ϕ_i) to $(0, 0)$, for $i = 1, 2, \dots, k$. The remaining qubits, indexed by $n+i$ for $i = 1, 2, \dots, k$, on Alice's and Bob's sides form k distilled Bell states, targeting the state $|\Phi^+\rangle$.

The above describes a one-way entanglement distillation protocol. A two-way protocol can also be implemented, in which Bob verifies only whether the syndrome $\mathbf{S} = \mathbf{0}$ to determine whether the distillation succeeds or fails, then communicates the result to Alice. This protocol can tolerate more errors (up to $d-1$) but is probabilistic and requires two-way classical communication.

Derivation.— To derive the protocol, we consider a setup consisting of n rows of qubits, as shown in Figure 2(a). Each row represents an entanglement swapping

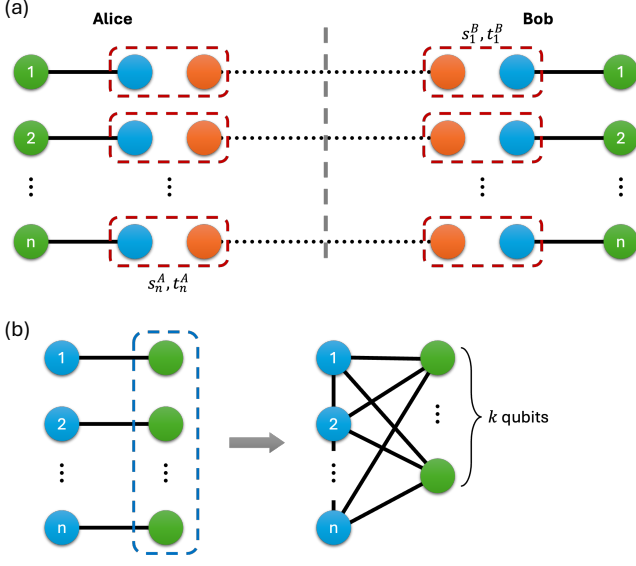


FIG. 2. (a) Schematic of n entanglement swapping processes, transferring entanglement from orange qubits shared between Alice and Bob to green qubits via Bell measurements. (b) Deriving the resource state by applying stabilizer and single-qubit measurements on the green qubits of local Bell states. The resulting states form logical-physical Bell states, with the blues qubits encoding k logical qubits.

process, where the connected green and blue circles represent local Bell states, and the orange circles represent a shared Bell state between Alice and Bob distributed over a noisy channel, all initialized in the standard Bell state

$$|\Phi^+\rangle = \frac{1}{\sqrt{2}} (|00\rangle + |11\rangle).$$

Alice and Bob perform Bell Measurements on the blue and orange qubits, yielding outcomes $s_i^{A(B)}$ for the XX -parity and $t_i^{A(B)}$ for the ZZ -parity, where i labels the row. Through these operations, the entanglement is swapped from the orange qubits to the green qubits, subject to local Pauli corrections. Using the stabilizer formalism [44], the standard Bell state can be represented by stabilizer generators $\{XX, ZZ\}$. After the measurements, the entangled green qubits are described by the stabilizers

$$\left\{ (-1)^{s_i} X_i \otimes X_i, (-1)^{t_i} Z_i \otimes Z_i \right\}, \quad (6)$$

where $s_i = s_i^A + s_i^B$ and $t_i = t_i^A + t_i^B$, and $i = 1, 2, \dots, n$. The \otimes symbol indicates the bilateral tensor product, with $O_A \otimes O_B$ denoting operators O_A and O_B acting on Alice's and Bob's sides, respectively.

We distill the n entangled states formed by the green qubits into k output states in the standard Bell states using an $[[n, k, d]]$ quantum error-correcting code. The distillation method follows the stabilizer-based entanglement distillation protocol described in detail in [18]. This

involves: (1) encoding the n entangled states into k logical Bell states through bilateral stabilizer measurements, and (2) decoding the logical states back into physical states using single-qubit measurements.

Given the n entangled states described in Equation 6, Alice and Bob perform $n - k$ stabilizer measurements on their qubits, resulting in outcomes a_i and b_i , respectively. These bilateral stabilizer measurements project the n entangled states into k logical entangled states, characterized by stabilizers

$$\left\{ \begin{array}{l} (-1)^{a_i} g_i \otimes I, \\ (-1)^{b_i} I \otimes g_i, \\ (-1)^{\phi_j} \bar{X}_j \otimes \bar{X}_j, \\ (-1)^{\beta_j} \bar{Z}_j \otimes \bar{Z}_j \end{array} \right\}, \quad (7)$$

for $i = 1, 2, \dots, n - k$ and $j = 1, 2, \dots, k$. The measurement outcomes a_i and b_i are random because the code stabilizers $g_i \otimes I$ and $I \otimes g_i$ anti-commute with $X_j \otimes X_j$ or $Z_j \otimes Z_j$ for any j -th qubit within the support of the stabilizer. However, their sum, representing the parity of $g_i \otimes g_i$, is fixed and determined by a linear combination of $X_j \otimes X_j$ and $Z_j \otimes Z_j$ over the supports of $g_i \otimes g_i$, expressed as

$$a_i + b_i = \mathbf{H}_1(i) \cdot \mathbf{s} + \mathbf{H}_2(i) \cdot \mathbf{t} + \mathbf{H}_1(i) \cdot \mathbf{H}_2(i)^T, \quad (8)$$

where $(\mathbf{H}_1(i) | \mathbf{H}_2(i))$ is the binary vector representation of g_i (the i -th row of the parity check matrix \mathbf{H}), and $\mathbf{H}_1(i) \cdot \mathbf{H}_2(i)^T$ accounts for the number of Pauli- Y components in g_i . These components contribute additional -1 due to $Y \otimes Y = -XZ \otimes XZ$. Since a_i and b_i are random, Alice and Bob post-select on both outcomes being 0, enforcing that the right-hand side (RHS) of Equation 8 equals 0. Errors in the transmitted orange qubits can flip Bell measurements \mathbf{s} and \mathbf{t} , altering the value of the RHS in Equation 8. This change reveals the error syndrome, as described in Equation 3. Similarly, Equations 4 and 5 are derived to compute the parities ϕ_j of $\bar{X}_j \otimes \bar{X}_j$ and β_j of $\bar{Z}_j \otimes \bar{Z}_j$ caused by Bell measurements and errors.

Given the logical Bell states in Equation 7, Alice and Bob can decode the logical states into physical states by performing $n - k$ single-qubit measurements [18]. For an $[[n, k, d]]$ stabilizer code, the measurement bases are chosen to map the logical operators \bar{X}_j and \bar{Z}_j to the physical operators $(-1)^{u_j} X_j$ and $(-1)^{w_j} Z_j$, respectively, for $j = 1, 2, \dots, k$. The phases u_j and w_j are linear functions of the measurement outcomes and can be set to 0 by post-selection. The decoded states are stabilized by

$$\left\{ (-1)^{\phi_j} X_j \otimes X_j, (-1)^{\beta_j} Z_j \otimes Z_j \right\}.$$

Bob then applies Pauli gates to correct any residual phases, yielding k standard Bell states.

The resource state remains to be derived. As shown in Figure 2, entanglement swapping and distillation are performed on different qubits, allowing their order to be

interchanged. The resource state is prepared by applying stabilizer and single-qubit measurements on the green qubits, which initially forms standard Bell states with the blue qubits. Post-selecting measurement outcomes of all 0s yields the resource state, with its stabilizers defined in Equation 1. Importantly, this post-selection is purely conceptual; in practice, the resource state can be prepared deterministically according to its stabilizers.

Measurement-based quantum repeaters.— Distributing high-fidelity Bell states over long distances requires quantum repeaters, which can be implemented using a measurement-based approach, as illustrated in Figure 3. The total distance is divided into N segments with $N+1$ nodes, where neighboring nodes share noisy Bell states (orange circles). Nodes 0 and N mark the end nodes, while intermediate nodes, labeled 1 through $N-1$, function as quantum repeaters. Each intermediate node performs Bell measurements using a resource state (blue and purple circles) derived from an $[[n, k, d]]$ -quantum error-correcting code. This enables the swapping of entanglement of k logical qubits between neighboring nodes while applying error correction. The quantum repeaters thus relay the logical Bell states, establishing entanglement between nodes 0 and N . At the end nodes, measurement-based entanglement distillation transforms the logical Bell states into physical Bell states (green circles).

We outline the repeater protocol below, considering two neighboring repeater nodes r and $r+1$, also referred to as Alice and Bob, respectively, as shown in Figure 3.

Step 1: Alice and Bob prepare their resource states, a $2n$ -qubit stabilizer state with generators

$$\{g_i, g'_i, \bar{X}_j \bar{X}'_j, \bar{Z}_j \bar{Z}'_j\} .$$

Here, g_i and g'_i , for $i = 1, 2, \dots, n-k$, represent the code stabilizer generators, acting on the blue and green qubits, respectively. $\bar{X}_j \bar{X}'_j$ and $\bar{Z}_j \bar{Z}'_j$ denote the tensor products of Pauli operators for the corresponding j -th logical qubits, where $j = 1, 2, \dots, k$. The resource state forms k logical Bell states, represented by

$$|\mathcal{R}_S\rangle = \frac{1}{\sqrt{2^k}} \bigotimes_{j=1}^k (|\bar{0}_j\rangle |\bar{0}'_j\rangle + |\bar{1}_j\rangle |\bar{1}'_j\rangle) . \quad (9)$$

Steps 2–4 mirror those in the distillation protocol, establishing logical Bell states between Alice’s blue qubits and Bob’s purple qubits. Bob then determines the bit flips $\beta^{(r)}$ and phase flips $\phi^{(r)}$ in the resulting state using Equations 4 and 5, accounting for the effects of errors and measurements.

Step 5: Each node transmits its computed bit and phase flips to the end node N , which determines the overall flips as $\beta = \sum_{r=1}^N \beta^{(r)}$ and $\phi = \sum_{r=1}^N \phi^{(r)}$, with summation performed modulo 2. Node N then applies the appropriate Pauli gates to its green qubits to correct these accumulated errors, transforming

(β_i, ϕ_i) to $(0, 0)$ for $i = 1, 2, \dots, k$. Consequently, k high-fidelity physical Bell states are established between Node 0 and N .

Quantum repeaters relay logical Bell states across nodes, analogous to storing logical quantum memories over time. Each segment effectively teleports logical Bell states while applying quantum error correction, akin to an error correction cycle for quantum memories. Given that neighboring nodes share noisy Bell states with fidelity \mathcal{F} , the infidelity $p = 1 - \mathcal{F}$ represents the physical qubit error rate. Quantum error correction reduces this, yielding a logical error rate p_L dependent on p and the chosen error-correcting code. The infidelity of the distributed Bell states between the end nodes, due to accumulated logical errors, is approximated by $(1 - p_L)^N \approx 1 - Np_L$ for small p_L .

Noisy Resource States.— The previous discussion assumes that errors occur only in input Bell states, with other components ideal. Here, we extend it to include noise in resource states, Bell measurements, and recovery gates. The distillation resource state in Equation 2 generalizes the standard Bell state, forming k logical-physical Bell states

$$|\Phi_D^+\rangle = \frac{1}{\sqrt{2}} (|\bar{0}\rangle |0\rangle + |\bar{1}\rangle |1\rangle) .$$

The logical subsystem consists of n interfacing qubits, each paired with an input qubit for a Bell measurement. Noise on these qubits affects measurement outcomes and can be mapped onto the input qubits [18, 36]. The physical subsystem consists of k output qubits, where noise can commute through distillation and act on the output Bell states. The Bell-state matrix identity [19],

$$(\bar{M} \otimes I) |\Phi_D^+\rangle = (I \otimes M^T) |\Phi_D^+\rangle , \quad (10)$$

transfers an operator \bar{M} acting on the logical subsystem to its transpose M^T on the physical subsystem. This enables the mapping of logical errors from interfacing qubits to output qubits, facilitating the evaluation of distillation capability. Assuming a depolarizing noise probability p per qubit, the interfacing qubits form a quantum error-correcting code that corrects physical errors, yielding a logical error rate p_L . Mapping this error to the output qubit using Equation 10 yields a modified output noise $O(p_L + p)$, which determines the distillation capability. Similarly, the repeater resource state in Equation 9 forms k logical-logical Bell states

$$|\Phi_S^+\rangle = \frac{1}{\sqrt{2}} (|\bar{0}\rangle |\bar{0}\rangle + |\bar{1}\rangle |\bar{1}\rangle) .$$

While physical errors are corrected, the remaining logical errors accumulate linearly as they propagate through the repeaters and can be analyzed using Equation 10. Noise in Bell measurements leads to flipped outcomes that can be mapped onto input qubits as bit and phase flip errors. In addition, errors in recovery gates directly affects the

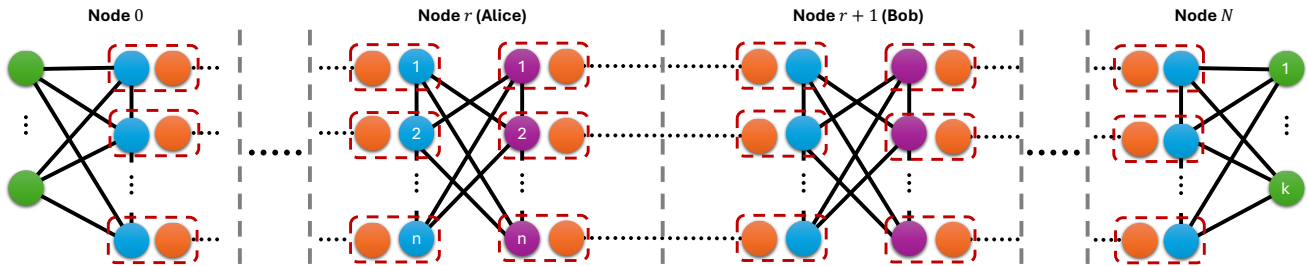


FIG. 3. Schematic of high-fidelity Bell state distribution over long distances using measurement-based quantum repeaters. The total distance is divided into N segments with $N + 1$ nodes. Intermediate nodes perform Bell measurements (dashed red rectangles) on input Bell states (orange circles) and resource states (blue and purple circles) derived from an $[[n, k, d]]$ -quantum error-correcting code, relaying entanglement to establish Bell states (green circles) between the end nodes.

output Bell states. This framework enables the analysis of measurement-based distillation and repeater protocols, incorporating noise components in the same manner as the ideal protocol but with modified errors on the input and output Bell states.

Since the resource states form logical-physical and logical-logical Bell states, their preparation simplifies to encoding logical Bell states. A promising approach [18] is to first locally prepare n copies of physical Bell states and then use bilateral stabilizer measurements to encode them onto logical Bell states, forming the repeater resource state. To obtain the distillation resource state, one can decode one part of the logical Bell state using single-qubit measurements. For certain codes, such as QLDPC codes, this preparation method features a constant circuit depth. Preserving the distillation resource state involves two components. The logical subsystems are protected via syndrome error correction. The physical systems can be stabilized using $\bar{X}X$ and $\bar{Z}Z$ measurements. However, as their weight increases with code distance, these measurements become inefficient. A more practical approach is to locally distill logical-physical Bell states [18], avoiding large-weight stabilizer measurements. Preserving the repeater resource state is more straightforward, as the logical subsystems can be independently corrected by syndrome error correction.

Quantum repeaters with constant yield rate.— We propose a measurement-based quantum repeater protocol using quantum low-density parity-check (QLDPC) codes for fault-tolerant Bell state distribution at a constant yield rate over any distance. These codes have a constant number of qubits per stabilizer generator and a constant number of generators per qubit, enabling efficient resource state preparation [18]. They also maintain a constant encoding rate and good code distance, exponentially suppressing logical errors [45, 46]. For $[[n, k = rn, d = O(\sqrt{n})]]$ -hypergraph product (HGP) codes with constant rate r [47], the logical error rate is given by [28]

$$p_L = c \left(\frac{p}{p_0} \right)^{\alpha n^\beta}, \quad (11)$$

where p is the physical error rate, p_0 is the error threshold, and α , β , and c are positive constants. To distribute Bell states over distance L , we divide it into segments of length L_0 , keeping neighboring-node Bell state infidelity below threshold. Each node then uses $2n$ -qubit resource states to fault-tolerantly relay the entanglement. Consequently, the end-to-end Bell state infidelity is

$$\frac{cL}{L_0} \left(\frac{p}{p_0} \right)^{\alpha n^\beta}.$$

Any target fidelity can be achieved by increasing the code size n while keeping the encoding rate r fixed, with n scaling polylogarithmically as $n = O(\log^{1/\beta} L)$.

We simulate the measurement-based entanglement distillation protocol using a family of HGP codes. Following the procedure outlined in previous literature [28, 48, 49], we construct HGP codes by taking the hypergraph product of classical (3, 4)-regular LDPC codes [47], which are randomly generated using software [50]. From the generated instances, we select the code with the maximal distance. By increasing the code size, we obtain a family of HGP codes with a constant encoding rate of 0.04. We then simulate the protocol using Stim [51] with belief propagation-ordered statistics decoding (BP-OSD) [48, 52, 53]. In our simulation, we assume that the input Bell states are noisy Werner states, while all other components, including resource states, Bell measurements, and recovery gates, are ideal.

Figure 4 shows the output Bell state infidelity p_{out} as a function of the input infidelity p_{in} for various code sizes. Due to finite-size effects in randomly generated codes, the 1225-code and 900-code share the same code distance. While it may seem unintuitive that the 1225-code outperforms the 900-code despite its larger size and identical distance, this is because error-correcting performance depends not only on the minimum weight but also on its overall distribution across codewords. We fit the data using Equation 11, obtaining an infidelity threshold of 9.3%, below which distillation improves the quality of the Bell state. Additionally, increasing the code size further enhances distillation performance. This result

- M. Van den Nest, Measurement-based quantum computation, *Nature Physics* **5**, 19 (2009).
- [12] Y. Li and S. C. Benjamin, High threshold distributed quantum computing with three-qubit nodes, *New Journal of Physics* **14**, 093008 (2012).
- [13] X.-M. Hu, Y. Guo, B.-H. Liu, C.-F. Li, and G.-C. Guo, Progress in quantum teleportation, *Nature Reviews Physics* **5**, 339 (2023).
- [14] H.-J. Briegel, W. Dür, J. I. Cirac, and P. Zoller, Quantum repeaters: The role of imperfect local operations in quantum communication, *Phys. Rev. Lett.* **81**, 5932 (1998).
- [15] L. Hartmann, B. Kraus, H.-J. Briegel, and W. Dür, Role of memory errors in quantum repeaters, *Phys. Rev. A* **75**, 032310 (2007).
- [16] L. Jiang, J. M. Taylor, K. Nemoto, W. J. Munro, R. Van Meter, and M. D. Lukin, Quantum repeater with encoding, *Phys. Rev. A* **79**, 032325 (2009).
- [17] S. H. Choe and R. König, Long-range data transmission in a fault-tolerant quantum bus architecture, *npj Quantum Information* **10**, 132 (2024).
- [18] Y. Shi, A. Patil, and S. Guha, Stabilizer entanglement distillation and efficient fault-tolerant encoder (2024), [arXiv:2408.06299 \[quant-ph\]](https://arxiv.org/abs/2408.06299).
- [19] M. M. Wilde, H. Krovi, and T. A. Brun, Convolutional entanglement distillation (2007), [arXiv:0708.3699 \[quant-ph\]](https://arxiv.org/abs/0708.3699).
- [20] W. Dür and H. J. Briegel, Entanglement purification and quantum error correction, *Reports on Progress in Physics* **70**, 1381 (2007).
- [21] C. H. Bennett, D. P. DiVincenzo, J. A. Smolin, and W. K. Wootters, Mixed-state entanglement and quantum error correction, *Phys. Rev. A* **54**, 3824 (1996).
- [22] R. Raussendorf and H. J. Briegel, A One-Way Quantum Computer, *Phys. Rev. Lett.* **86**, 5188 (2001).
- [23] M. Zwerger, W. Dür, and H. J. Briegel, Measurement-based quantum repeaters, *Phys. Rev. A* **85**, 062326 (2012).
- [24] D. L. Moehring, M. J. Madsen, K. C. Younge, J. R. N. Kohn, P. Maunz, L.-M. Duan, C. Monroe, and B. B. Blinov, Quantum networking with photons and trapped atoms (invited), *J. Opt. Soc. Am. B* **24**, 300 (2007).
- [25] P. Dhara, N. M. Linke, E. Waks, S. Guha, and K. P. Seshadreesan, Multiplexed quantum repeaters based on dual-species trapped-ion systems, *Phys. Rev. A* **105**, 022623 (2022).
- [26] A. Kang, S. Guha, N. Rengaswamy, and K. P. Seshadreesan, Trapped ion quantum repeaters with entanglement distillation based on quantum ldpc codes, in *2023 IEEE International Conference on Quantum Computing and Engineering (QCE)*, Vol. 01 (2023) pp. 1165–1171.
- [27] D. Bluvstein, S. J. Evered, A. A. Geim, S. H. Li, H. Zhou, T. Manovitz, S. Ebadi, M. Cain, M. Kalinowski, D. Hangleiter, J. P. Bonilla Ataides, N. Maskara, I. Cong, X. Gao, P. Sales Rodriguez, T. Karolyshyn, G. Semeghini, M. J. Gullans, M. Greiner, V. Vuletić, and M. D. Lukin, Logical quantum processor based on reconfigurable atom arrays, *Nature* **626**, 58 (2024).
- [28] Q. Xu, J. P. Bonilla Ataides, C. A. Pattison, N. Raveendran, D. Bluvstein, J. Wurtz, B. Vasić, M. D. Lukin, L. Jiang, and H. Zhou, Constant-overhead fault-tolerant quantum computation with reconfigurable atom arrays, *Nature Physics* [10.1038/s41567-024-02479-z](https://doi.org/10.1038/s41567-024-02479-z) (2024).
- [29] C. A. Pattison, G. Baranes, J. P. B. Ataides, M. D. Lukin, and H. Zhou, Fast quantum interconnects via constant-rate entanglement distillation (2024), [arXiv:2408.15936 \[quant-ph\]](https://arxiv.org/abs/2408.15936).
- [30] N. Constantinides, A. Fahimniya, D. Devulapalli, D. Bluvstein, M. J. Gullans, J. V. Porto, A. M. Childs, and A. V. Gorshkov, Optimal routing protocols for reconfigurable atom arrays (2024), [arXiv:2411.05061 \[quant-ph\]](https://arxiv.org/abs/2411.05061).
- [31] K. Azuma, K. Tamaki, and H.-K. Lo, All-photon quantum repeaters, *Nature Communications* **6**, 6787 (2015).
- [32] B. Li, S. E. Economou, and E. Barnes, Photonic resource state generation from a minimal number of quantum emitters, *npj Quantum Information* **8**, 11 (2022).
- [33] A. Patil and S. Guha, An improved design for all-photon quantum repeaters (2024), [arXiv:2405.11768 \[quant-ph\]](https://arxiv.org/abs/2405.11768).
- [34] R. A. Parker, J. Arjona Martínez, K. C. Chen, A. M. Stramma, I. B. Harris, C. P. Michaels, M. E. Trusheim, M. Hayhurst Appel, C. M. Purser, W. G. Roth, D. Englund, and M. Atatüre, A diamond nanophotonic interface with an optically accessible deterministic electronuclear spin register, *Nature Photonics* **18**, 156 (2024).
- [35] H. K. Beukers, M. Pasini, H. Choi, D. Englund, R. Hanson, and J. Borregaard, Remote-entanglement protocols for stationary qubits with photonic interfaces, *PRX Quantum* **5**, 010202 (2024).
- [36] M. Zwerger, H. J. Briegel, and W. Dür, Universal and optimal error thresholds for measurement-based entanglement purification, *Phys. Rev. Lett.* **110**, 260503 (2013).
- [37] A. Jamiolkowski, Linear transformations which preserve trace and positive semidefiniteness of operators, *Reports on Mathematical Physics* **3**, 275 (1972).
- [38] M. Zwerger, A. Pirker, V. Dunjko, H. J. Briegel, and W. Dür, Long-range big quantum-data transmission, *Phys. Rev. Lett.* **120**, 030503 (2018).
- [39] N. P. Breuckmann and J. N. Eberhardt, Quantum low-density parity-check codes, *PRX Quantum* **2**, 040101 (2021).
- [40] W. Dür, H. Aschauer, and H.-J. Briegel, Multiparticle entanglement purification for graph states, *Phys. Rev. Lett.* **91**, 107903 (2003).
- [41] M. Nielsen and I. Chuang, *Quantum Computation and Quantum Information: 10th Anniversary Edition* (Cambridge University Press, 2010).
- [42] A. Calderbank, E. Rains, P. Shor, and N. Sloane, Quantum error correction via codes over $gf(4)$, *IEEE Transactions on Information Theory* **44**, 1369 (1998).
- [43] M. Hein, J. Eisert, and H. J. Briegel, Multiparty entanglement in graph states, *Phys. Rev. A* **69**, 062311 (2004).
- [44] D. Gottesman, Stabilizer codes and quantum error correction (1997), [arXiv:quant-ph/9705052 \[quant-ph\]](https://arxiv.org/abs/quant-ph/9705052).
- [45] D. Gottesman, Fault-tolerant quantum computation with constant overhead, *Quantum Info. Comput.* **14**, 1338–1372 (2014).
- [46] N. Rengaswamy, N. Raveendran, A. Raina, and B. Vasić, Entanglement Purification with Quantum LDPC Codes and Iterative Decoding, *Quantum* **8**, 1233 (2024).
- [47] J.-P. Tillich and G. Zémor, Quantum ldpc codes with positive rate and minimum distance proportional to the square root of the blocklength, *IEEE Transactions on Information Theory* **60**, 1193 (2014).
- [48] J. Roffe, D. R. White, S. Burton, and E. Campbell, Decoding across the quantum low-density parity-check code

- landscape, *Phys. Rev. Res.* **2**, 043423 (2020).
- [49] A. Grospellier, L. Grouès, A. Krishna, and A. Leverrier, Combining hard and soft decoders for hypergraph product codes, *Quantum* **5**, 432 (2021).
- [50] R. Prabhakar, S. Chandak, and K. Tatwawadi, [Implementation of protograph ldpc error correction codes](#) (2020).
- [51] C. Gidney, Stim: a fast stabilizer circuit simulator, *Quantum* **5**, 497 (2021).
- [52] J. Roffe, [LDPC: Python tools for low density parity check codes](#) (2022).
- [53] P. Panteleev and G. Kalachev, Degenerate Quantum LDPC Codes With Good Finite Length Performance, *Quantum* **5**, 585 (2021).
- [54] J. P. B. Ataiades, H. Zhou, Q. Xu, G. Baranes, B. Li, M. D. Lukin, and L. Jiang, [Constant-overhead fault-tolerant bell-pair distillation using high-rate codes](#) (2025), [arXiv:2502.09542 \[quant-ph\]](#).